Nanoscale

PAPER

View Article Online
View Journal | View Issue

Cite this: *Nanoscale*, 2025, **17**, 13756

Thienothiophene-based quantum dots: calibration of photophysical properties *via* carbon dot and biomolecular interactions†

Recep Isci, *[a] Ozge Ibis,[a] Garen Suna,[a] Caner Unlu *[a] and Turan Ozturk *[a,b]

Received 6th March 2025,
Accepted 12th May 2025

DOI: 10.1039/d5nr00980d

rsc.li/nanoscale

Semiconductor-based quantum dots (QDs) are size-tunable, photostable and extremely effective fluorophores with strong bandgap luminescence, which make them attractive for biological and medical nano-applications. Herein, we present a thienothiophene (TT)-based highly conjugated fluorescent semiconductor containing triphenylamine (TPA) and tetraphenylethylene (TPE) units, **TT-TPE-TPA**, as a QD conjugate. As **TT-TPE-TPA** exhibits remarkable photophysical properties such as a maximum solid-state quantum yield of 47%, a maximum fluorescence solution quantum yield of 81%, a mega Stokes shift of 133 nm and a positive solvatochromism from blue to orange colors, its carbon–nitrogen (CN) and carbon–nitrogen–boron (CNB) dots were prepared. While the dots changed the emission characteristics of **TT-TPE-TPA**, depending on the enhanced conjugation and fluorescence properties of **TT-TPE-TPA**/CDs, tunable optical properties were achieved towards vital biomolecules such as urea, NH_4Cl and sucrose. By systematically modulating the composition and concentration of **TT-TPE-TPA**, CDs, and biomolecules, the detailed mechanisms of energy transfer, fluorescence quenching, and radiation enhancement were revealed. This work opens the door to a new class of promising optical nanomaterials that could be controlled in TT-based QDs.

1. Introduction

Recently, fluorescent nanoparticles have emerged as a significant research subject with applications in many optoelectronic and imaging technologies.[1–3] By far, the most popular fluorescent nanoparticles are primarily based on metals, semiconductors and metal oxides, among which semiconductor-based quantum dots (QDs) have received increasing attention owing to their unique electronic and optical properties such as photostability, tunability and high brightness.[4–8] Recently, QDs with prominent lifetime and photo-bleaching resistivity properties have been intensively studied, especially in sustainable optoelectronics such as bioimaging, photodetection, drug delivery and diagnostic fields.[9–11] QDs and π-conjugated molecules with semiconducting properties have enabled novel functional hybrid materials for controlling the energy and/or charge transfer properties of optical nanomaterials.[11–13] These properties make them highly sensitive toward various biomolecules exhibiting a fluorescence signal response.[14–17] Among conjugated structures, thiophene derivatives, in particular, are of significant interest for QDs because of their ideal optical, electrical and electro-/photoluminescence properties. Various thiophene-based materials have enhanced electron injection and improved carrier balance, serving as organic ligands, nanoparticles and nanocomposites in the device architecture of QDs.[18–20]

Thieno[3,2-*b*]thiophene (TT) and its derivatives are among the most prominent and widely used compounds as part of the thiophene family for organic semiconductors. TT has a flat and highly pi-conjugated rigid structure, making it a suitable π-spacer for tuning the electronic band gap, enabling intermolecular interactions in the solid state, and developing building blocks of various organic materials.[21–27] Electron-rich properties of TT and its derivatives make them promising candidates for the development of organic electronics and optoelectronics such as organic solar cells, perovskites, photoinitiators, supercapacitors, organic light-emitting diodes, organic field-effect transistors, phototransistors and sensors.[28–36] Triphenylamine (TPA) is an important fluorophore with an ionization potential of 6.80 eV and sp^2 hybridization, which make it a strong electron donor unit in many optical applications.[37–40] Tetraphenylethylene (TPE) is known as a

[a]*Istanbul Technical University, Chemistry Department, 34469 Maslak, Istanbul, Turkey. E-mail: isci@itu.edu.tr*
[b]*TUBITAK UME, Chemistry Group Laboratories, 41470 Gebze, Kocaeli, Turkey*
† Electronic supplementary information (ESI) available. See DOI: https://doi.org/10.1039/d5nr00980d

non-emissive chromophore in solutions and highly emissive in the solid state considering its twisted structure, resulting in intramolecular restriction.[41–44]

In this work, a multifunctional TT-based fluorophore, **TT-TPE-TPA**, incorporating TPE and TPA groups at the peripherals of the TT core, was synthesized, which had an extensive conjugation, particularly through TPA and highly emissive properties in the solid state provided by the restricted intramolecular motions of TPE. Its photophysical properties were investigated by UV-Vis and fluorescence spectroscopies, which displayed remarkable photophysical features such as a mega Stokes shift of 109 nm, high fluorescence quantum yields both in solid state (47%) and in solution (81%) and a positive solvatochromic charge transfer behavior with the changing polarity index. Considering its outstanding optical properties, QD hybrids of **TT-TPE-TPA** were prepared. Carbon–nitrogen (CN)- and carbon–nitride–boron (CNB)-based **TT-TPE-TPA** dots were processed and their biomolecular interactions were systematically investigated on the conjugate-biomolecule case. The carbon dots altered the photophysical properties of **TT-TPE-TPA** after conjugation by changing the emission and excitation characteristics of **TT-TPE-TPA**. CN and CNB CDs exhibited distinct effects on photophysical properties. In addition, creating a further conjugation with selected biomolecules, *i.e.* urea, NH_4Cl and sucrose, the photophysical properties of **TT-TPE-TPA**/CD conjugates proved to be excellent candidates for further modulation with various reagents.

2. Experimental

2.1 Materials

n-Butyllithium (2.5 M in hexane, Across), tributyltin chloride (96%, Sigma-Aldrich), tetrakis(triphenylphosphine)palladium (0) ($Pd(PPh_4)_3$) (99%, Sigma-Aldrich), hydroquinone 99% (Across) and anhydrous sodium sulfate (99%, Sigma-Aldrich) were obtained from commercial sources and used without further purification unless otherwise mentioned. Dry THF and toluene were obtained *via* distillation over sodium/benzophenone. Dimethylformamide (HPLC grade) was stored over activated molecular sieves (4 Å). Dichloromethane (Aldrich) was used as received. For carbon dot synthesis and interaction studies, dimethylformamide (DMF, 99.8%, VWR Chemicals), citric acid monohydrate (Aldrich), boric acid (99.5% Aldrich), urea (Aldrich), ammonium chloride (NH_4Cl, 99.5%, Aldrich) and industrial sugar sucrose (table sugar) were used without further purification.

2.2 Synthesis of *N*,*N*-diphenyl-4-(5-(tributylstannyl)thiophen-2-yl)aniline (8)

To *N*,*N*-diphenyl-4-(thiophen-2-yl)aniline (6.1 mmol, 2.0 g) dissolved in dry THF (50 mL) was added *n*-BuLi (6.70 mmol, 4.19 mL, 1.6 M) dropwise under a nitrogen atmosphere at −78 °C. After stirring for one hour at the same temperature, tributylchlorostannane (12.2 mmol, 12.2 mL, 1.0 M) was added and the stirring was continued for further 24 h. The reaction mixture was then extracted with DCM and water. The organic phase was dried over Na_2SO_4 and filtered, and the solvent was evaporated under reduced pressure. The crude product was used in the subsequent reaction without further purification.

2.3 Synthesis of TT-TPE-TPA

To a mixture of **5** (480 μmol, 300 mg) and **8** (620 μmol, 380 mg), dissolved in toluene (30 mL) and then degassed, was added $Pd(PPh_3)_4$ (27.0 mg, 5 mol%) under a nitrogen atmosphere. The mixture was refluxed for 48 h and filtered through Celite to remove the metal catalyst, and the solvent was evaporated under reduced pressure. The crude product was purified by column chromatography using silica gel as a packing agent and an *n*-hexane/DCM (8 : 1) mixture as an eluent, which gave a yellow solid in 79% (330 mg) yield. ^{1}H NMR (500 MHz, $CDCl_3$) δ 7.65 (d, J = 8.3 Hz, 2H), 7.60 (d, J = 8.3 Hz, 2H), 7.44 (d, J = 8.3 Hz, 2H), 7.41–7.37 (m, 3H), 7.29–7.26 (m, 5H), 7.15–7.03 (m, 26H), 6.99 (d, J = 3.7 Hz, 1H). ^{13}C NMR (126 MHz, $CDCl_3$) δ 147.40, 144.82, 143.67, 143.05, 142.00, 141.20, 140.49, 140.09, 138.12, 136.11, 134.82, 133.85, 133.28, 131.87, 131.41, 131.34, 130.35, 129.50, 129.31, 127.91, 127.77, 127.69, 127.64, 127.16, 126.86, 126.46, 126.07, 124.54, 123.50, 123.15, 122.41, 119.74. MS m/z 872.6 (M + 1).

2.4 Synthesis of carbon dots

The carbon dots were produced following the microwave-assisted hydrothermal treatment method. Thus, an aqueous solution (30 mg mL^{-1}) of citric acid monohydrate, urea and boric acid was prepared.

To a solution of CN CDs, prepared as a mixture of citric acid monohydrate (3.33 mL) and urea (3.33 mL), was added distilled water (3.33 mL). The mixture was irradiated under 800 watt microwave power for 12 minutes in a household microwave oven. The produced brown carbon dots were dissolved in water (10 mL) and filtered twice, *i.e.* initially using filter paper (qualitative filter paper with 10 μm pore size) and then through membranes (0.22 μm). The final solution was dried at 45 °C, and the solid product was stored in a refrigerator for further use.

CNB CDs prepared as 3.33 ml of citric acid monohydrate solution, 3.33 ml of urea solution and 3.33 ml of boric acid solution were mixed in a flat-bottom flask and then irradiated under 800 watt microwave power for 12 minutes in a domestic microwave oven. The produced dark orange carbon dot was dissolved in 10 ml water and filtered twice through (i) qualitative filter paper with 10 μm pore size and then (ii) 0.22 μm membranes. The final solution was dried at 45 °C, and the solid product was stored in a refrigerator for further use.

2.5 TT-TPE-TPA/CD and TT-TPE-TPA/CD/biomolecule interactions

While **TT-TPE-TPA** (0.5 mg mL^{-1}), CN-dot (5 mg mL^{-1}) and CNB-dot (5 mg mL^{-1}) solutions were prepared in DMF, the biomolecules NH_4Cl, urea and table sugar, used for interactions, were prepared in distilled water at a concentration of 20 mg ml^{-1}.

TT-TPE-TPA was initially stirred with CN or CNB carbon dots for 2 h and then the biomolecule was introduced to the mixture. The stirring was continued further for 48 h at room temperature, after which the photoluminescence spectroscopy studies were conducted. Each experiment was performed 3 times to check the reproducibility and precision of the results. All results from the replicates were conclusive, showing only minor variation (5–7 percent).

3. Results and discussion

3.1 Design and synthesis

The TT and TPA derivatives (**2**–**7**) were synthesized following our previous reports.[35,36,40,46,41,45] Initially, the synthesis of the core unit, 3-(4-bromophenyl)thieno[3,2-*b*]thiophene **3**, was conducted starting from 3-bromothiophene (**1**). The monoketone, **2**, was constructed in a one-pot three-step reaction: (i) lithiation of 3-bromothiophene (**1**) with *n*-butyllithium at −78 °C, (ii) addition of elemental sulfur and (iii) 2-bromo-1-(4-bromophenyl)ethanone (**2**), in yield of 83%. Its ring closure was performed in the presence of polyphosphoric acid (PPA) in refluxing chlorobenzene to give **3** in 81% yield. The Suzuki coupling reaction of **3** with a boronated tetraphenylethylene unit produced the compound **4** (**TT-TPE**) in 79%. The brominated **TT-TPE**, **5**, was obtained through selective mono bromination of **4** using NBS at −10 °C in DMF in 81% yield. The Suzuki coupling reaction of **6** with boronated thiophene produced the thiophene-extended TPA, **7**, in a yield of 68%. It was stannylated by lithiation with *n*-butyllithium and then addition of tributyltin chloride to obtain **8**. The Stille coupling reaction of **5** with **8** produced the target compound **TT-TPE-TPA** in 79% yield (Scheme 1).

3.2 Photophysical properties

The photophysical properties (UV-Vis absorption and emission spectra) of **TT-TPE-TPA** were investigated in THF at room temperature (Table 1 and Fig. 1a). The maximum π–π* absorption wavelength (λ_{max}) of **TT-TPE-TPA** was measured to be 389 nm, from which the onset maximum of 459 nm was observed. Then, the optical band gaps were determined to be 2.68 eV. The fluorescence measurements in THF displayed emission maxima of 522 nm (Table 1 and Fig. 1a), demonstrating mega Stokes shifts of 133 nm, which could be due to efficient intra-

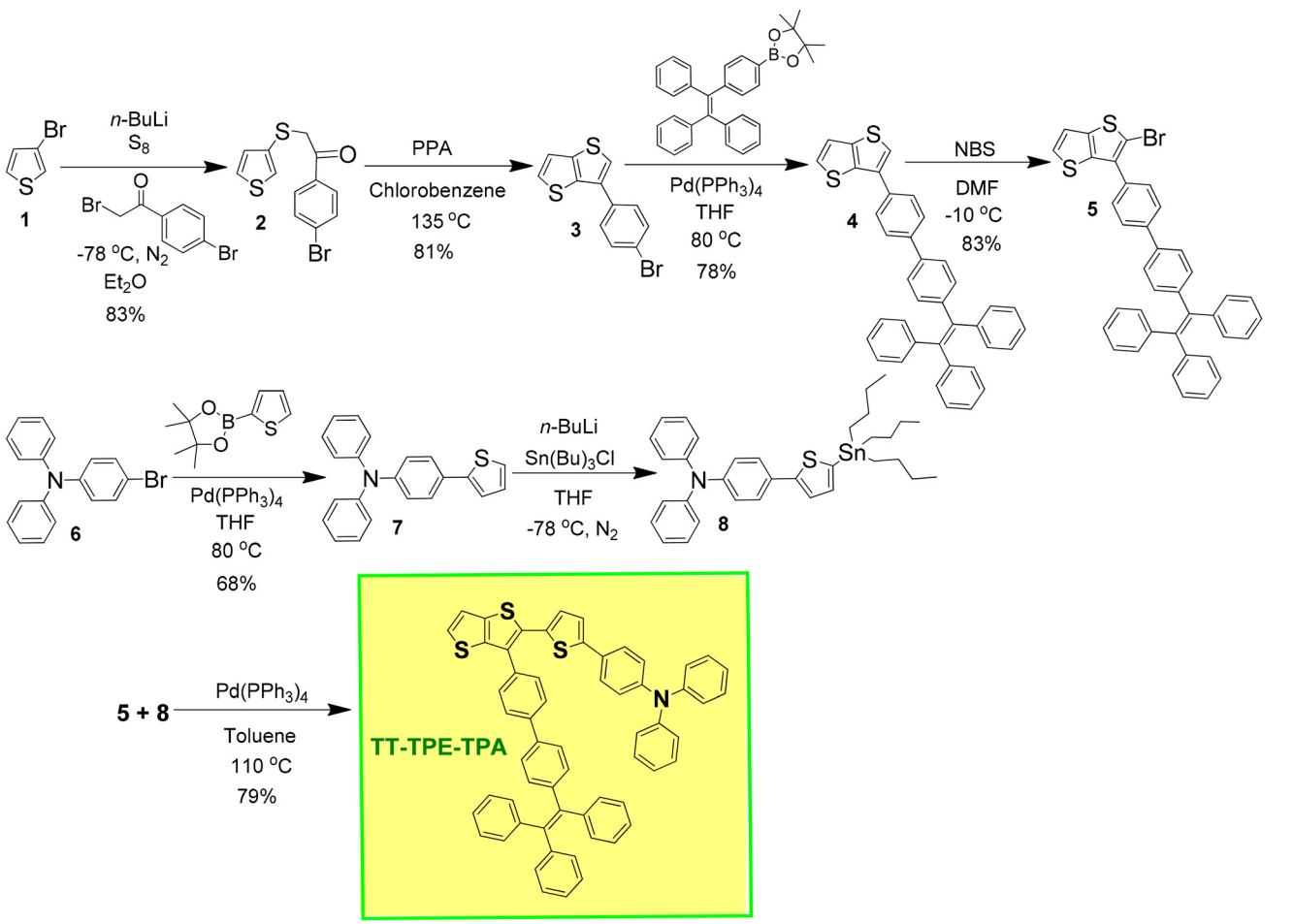

Scheme 1 Synthesis of **TT-TPE-TPA**.

Table 1 Photophysical data of **TT-TPE-TPA**

Compound	$\lambda_{abs,\ max}$ [a] (nm)	λ_{onset} [b] (nm)	$\lambda_{fl,\ max}$ [a] (nm)	Stokes shift (nm)	E_{opt} [c] (eV)	Q_{solid} [d] (%)	$Q_{solution}$ [e] (%)
TT-TPE-TPA	389	459	522	133	2.68	47	81

[a] Absorption and emission maximum in THF. [b] Onset of the absorption in THF. [c] $E_{optic} = hc/\lambda_{onset}$. [d] Solid-state quantum yield. [e] Solution-state quantum yield in THF.

molecular charge-transfer (ICT) between TT and TPA groups. Moreover, mega Stokes shifts of the compounds indicated a fast relaxation from the excited state to the ground state; owing to ICT, the materials are optically applicable. **TT-TPE-TPA** showed solid-state fluorescence, attributed to its restricted design, and while a maximum solid-state quantum yield was obtained to be 47%, the solution quantum efficiency reached 81% in THF.

In order to investigate the charge transfer nature of **TT-TPE-TPA** in detail, its solvatochromic behaviors were investigated in nine different solvents, having different polarities from polar to nonpolar, *i.e.* DMSO, DMF, acetonitrile, acetone, chloroform, dichloromethane, chlorobenzene, toluene and hexane (Table S1†). While it had no significant change in their absorption bands with the solvent polarity (Fig. S1†), **TT-TPE-TPA** displayed a bathochromic shift visible to naked eye in the emission spectra with increasing solvent polarity, indicating a strongly stabilized excited state through the surrounding solvents with remarkable charge transfer character and larger dipole moments compared to the ground state (Fig. 1b). The bathochromic shifts of 55 nm for **TT-TPE-TPA** with increasing polarity demonstrated its positive solvatochromic behavior. This difference in the shift showed that **TT-TPE-TPA** has a strong charge transfer property. Its possible explanation could be a high π-electron conjugation between TT and TPA units.

The influence of solvent polarity on fluorescence was investigated using a Lippert–Mataga plot, which is a plot of Stokes shift (ΔV in cm^{-1}) *vs.* orientation polarizability (Δf) of the solvent. It provided the solvent-dependent spectral shifts with a framework (Fig. 2a). **TT-TPE-TPA**, with a wide range of color emissions due to high π-conjugation, showed a positive solvatochromic trend as a solvent polarity indicator and a positive slope, indicating intramolecular charge transfer (ICT) with increasing Stokes shifts.

Considering all these dramatic photophysical properties, the molecular design of **TT-TPE-TPA** displayed strong charge transfer through extensive conjugation provided by the strong electron donor TPA having 6.80 eV ionization energy.[37,40] Furthermore, the incorporation of the TPE group, which is an AIE (aggregation induced emission) active group at the 3-position of TT, led to a restricted intramolecular motion and rigidity between TPA and TPE units,[37,41] resulting in a solid-state quantum yield of 47%.

3.3 Quantum dot properties and biomolecular interactions

Understanding and controlling the photophysical properties of conjugates, constructed by the combination of two different fluorophores, are critical for advancing applications in biosensing, imaging and optoelectronics. In this study, interactions between **TT-TPE-TPA**, carbon dots (CDs) and various biomolecules were systematically investigated. By adjusting the concentration and composition of these conjugates and considering structural elements like thienothiophene and the effects of biomolecular modulators, a balance between radiative and nonradiative transitions was observed.

In particular, the ability to control and fine-tune the photophysical properties of these conjugates offers significant

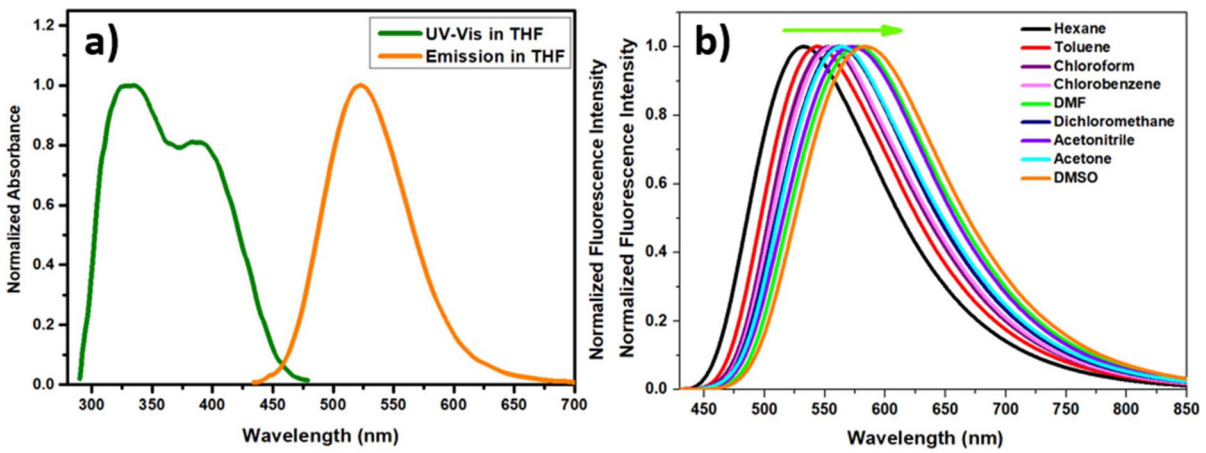

Fig. 1 (a) Absorption and emission spectra of **TT-TPE-TPA** in THF. (b) Photoluminescence spectra of **TT-TPE-TPA** in solvents with different polarities (from hexane to DMSO).

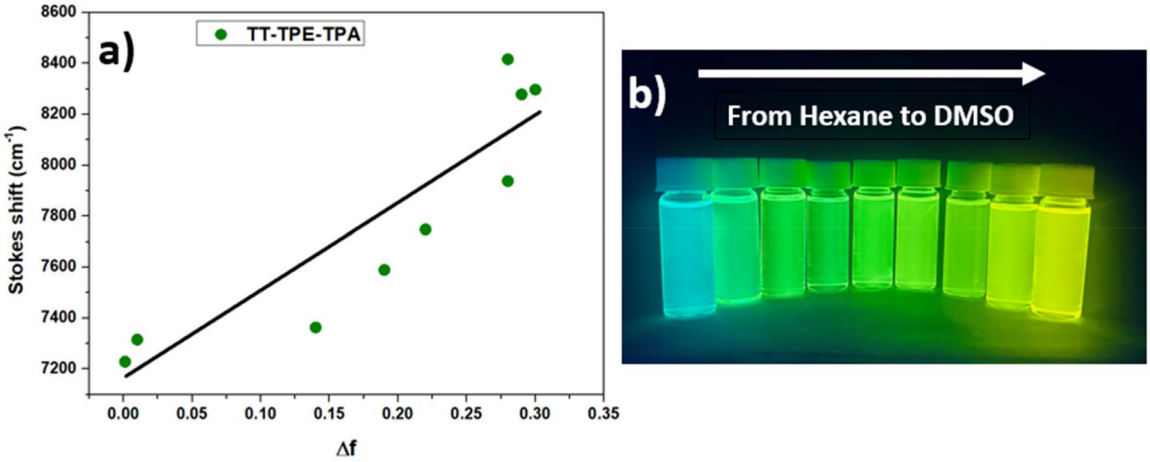

Fig. 2 (a) Lippert–Mataga plot for **TT-TPE-TPA** in different solvents showing the variation in Stokes shift as a function of the orientation polarizability of the solvents. (b) **TT-TPE-TPA** under UV light in different solvents.

opportunities in various biosensing and imaging platforms. For instance, the **TT-TPE-TPA-CD** systems with strong, environment-sensitive fluorescence can be integrated into real-time detection assays where shifts in emission wavelength or intensity report on specific analytes or physiological conditions. Such responsiveness is especially valuable for cellular imaging, where the local microenvironment (pH, ionic strength, and viscosity) may trigger a measurable change in emission. Additionally, the high biocompatibility of carbon dots further broadens their potential utility *in vivo*, enabling the development of targeted fluorescent probes that can illuminate molecular or structural features without adversely affecting their cellular function. These diverse uses point out the ways in which the mechanistic knowledge acquired herein, specifically with regard to sucrose-induced spectral shifts and biomolecule-responsive conjugate behavior, can direct the development of sophisticated, custom fluorophore-nanomaterial constructs for theranostics, diagnostics and other fields.

Each molecule, **TT-TPE-TPA** and CDs, exhibited distinct emission properties (Fig. 3). Upon excitation at 360 nm, **TT-TPE-TPA** produced a single Gaussian emission peak centered at 535 nm with a full width at half maximum (FWHM) of 100 nm. In contrast, both CN and CBN CDs exhibited emission peaks at shorter wavelengths. In particular, the CN CDs displayed a single emission peak with a maximum at 440 nm and an FWHM of 110 nm when excited at 350 nm, whereas the CBN CDs exhibited a single emission peak with a maximum at 445 nm and an FWHM of 80 nm. These emission characteristics are consistent with those reported in the literature.[47] In addition, the FTIR spectrum of each CD showed that the CDs had –COOH, $–NH_2$ and –OH groups on the surface, as observed for the same CDs reported in the literature (Fig. S2†).[47]

To investigate the interaction between **TT-TPE-TPA** and CDs, a series of conjugation experiments were conducted in which the CD concentration was gradually varied while maintaining a constant **TT-TPE-TPA** concentration (Fig. 4). In each experiment, the emission intensity of **TT-TPE-TPA** at 535 nm decreased gradually with the increase in CD concentration, indicating that **TT-TPE-TPA** interacts with the CDs leading to the quenching of emission of **TT-TPE-TPA**. Notably, the emission intensity of the CDs was also quenched with the increasing degree of quenching as the CD concentration increased. According to Beer–Lambert's law, in the absence of any interaction, the emission of the CDs should increase with the concentration. Therefore, the observed quenching suggested that the interaction between CDs and **TT-TPE-TPA** gave rise to new nonradiative energy states at the expense of radiative states, thereby reducing the overall emission intensity of the **TT-TPE-TPA-CD** conjugates. Furthermore, the impact of CDs

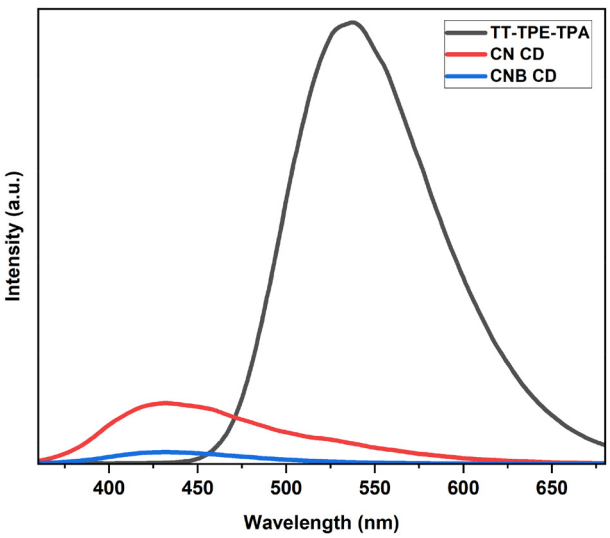

Fig. 3 Emission of **TT-TPE-TPA**, CN, and CBN CDs upon excitation at 350 nm in DMF.

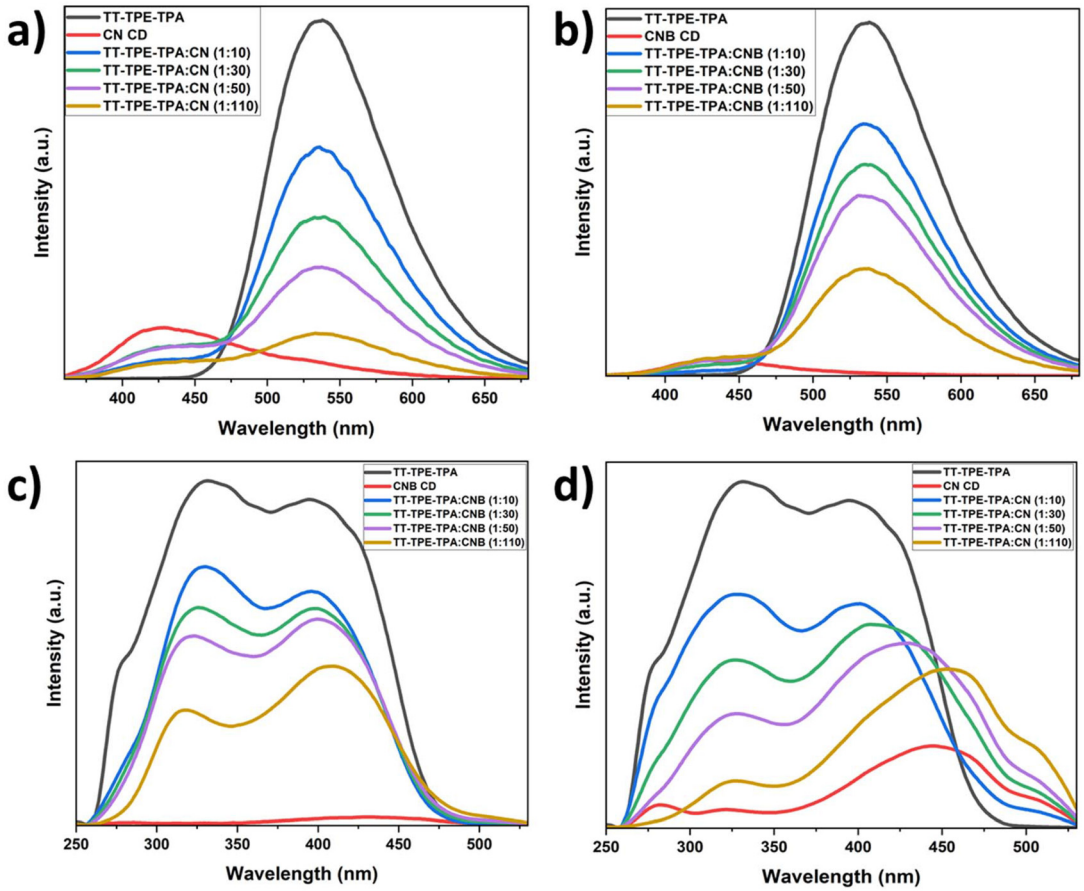

Fig. 4 Interaction of **TT-TPE-TPA** with CDs. (a) Change in the emission spectrum of **TT-TPE-TPA** with an increase in the concentration of CN CDs. The emission spectrum was recorded upon excitation at 350 nm. (b) Change in the emission spectrum of **TT-TPE-TPA** with an increase in the concentration of CNB CDs. The emission spectrum was recorded upon excitation at 350 nm. (c) Change in the photoluminescence excitation spectrum of **TT-TPE-TPA** with an increase in the concentration of CN CDs. The photoluminescence excitation spectrum was recorded at 535 nm emission. (d) Change in the photoluminescence excitation spectrum of **TT-TPE-TPA** with an increase in the concentration of CNB CDs. The photoluminescence excitation spectrum was recorded at 535 nm emission.

on the emission of **TT-TPE-TPA** differed between CN and CBN CDs. In particular, the emission of **TT-TPE-TPA** decreased more significantly upon interaction with CN CDs compared to CBN CDs. In particular, the incorporation of boron in the CBN CDs introduced hydroxyl groups on the surface, which may alter the surface charge and polarity and thus slightly disrupt and weaken the interaction between **TT-TPE-TPA** and the CDs.

To investigate the effect of CDs on the emission properties of **TT-TPE-TPA**, the photoluminescence excitation (PLE) spectra of **TT-TPE-TPA**, CDs and **TT-TPE-TPA-CD** conjugates were recorded. In PLE spectroscopy, the emission intensity is monitored as a function of the excitation wavelength, providing insights into the electronic transitions responsible for luminescence by identifying the wavelengths at which absorption leads to emission. The PLE spectrum was measured at 535 nm, corresponding to the emission maximum of **TT-TPE-TPA**, which exhibited three distinct peaks at 275, 325 and 415 nm with the intensities approximately equal to 325 and 415 nm and comparatively minor at 275 nm. These peaks were attributed to allowed π–π* transitions in the thiophene structure, *i.e.* the higher energy (shorter-wavelength) peaks corresponding to electronic transitions localized within the thiophene ring, whereas the lower energy (longer-wavelength) peak is associated with the transitions involving the entire system. Upon interaction with CDs, the intensities of the peaks at 275 and 325 nm decreased gradually with the increase in CD concentration, indicating suppression of the allowed radiative transitions associated with the thiophene ring. A similar trend was observed for the peak at 415 nm of the **TT-TPE-TPA-CBN** conjugate system, the intensity of which diminished progressively in the presence of CBN. These observations suggested that conjugation between **TT-TPE-TPA** and CBN led to a reduction in radiative transitions and the formation of nonradiative pathways, most probably due to ultrafast thermal relaxation processes. Regarding the **TT-TPE-TPA-CN** conjugate system, in contrast, the peak at 415 nm not only decreased in intensity but also exhibited a gradual bathochromic shift, implying that as the CN concentration increases, radiative transitions become increasingly dominant.

To have insights into how the conjugation of CDs with **TT-TPE-TPA** affected their interactions with biomolecules, the PLE spectra of **TT-TPE-TPA**, CDs and their conjugates were compared in the presence and absence of the three biomolecules, *i.e.* urea, sucrose, and ammonium chloride (NH_4Cl) (Fig. 5). These biomolecules were selected as they uniquely influence the interaction environment, thus providing a comprehensive platform for probing biomolecule–material interactions. Urea is known to disrupt hydrogen-bonding networks and induce biomolecular denaturation, enabling the evaluation of how altered hydrogen-bond stability affects nanomaterial binding.[48–51] In contrast, sucrose acts as an osmolyte that modulates the hydration shell and solvent dynamics of surrounding biomolecules, which is critical for assessing the roles of solvation effects and molecular crowding.[52] Additionally, NH_4Cl adjusts the ionic strength and pH of the system, thereby facilitating the investigation of electrostatic and charge-mediated forces at the nano-bio interface.[53] Together, these agents enable a systematic dissection of the physicochemical parameters governing biomolecule–material interactions.

The PLE spectra of the biomolecule-**TT-TPE-TPA**, biomolecule-CDs and biomolecule-conjugate systems were recorded at an emission wavelength of 535 nm to assess the effect of biomolecules on the photophysical properties of **TT-TPE-TPA** in the presence and absence of CDs. The PLE spectrum directly probes the absorption characteristics of the materials responsible for radiative transitions and is highly sensitive to local environmental changes induced by biomolecule binding. As the PLE technique monitors variations in the excitation profile, it can detect subtle shifts and quenching effects that might be obscured in the emission spectrum due to overlapping signals. Consequently, PLE serves as a superior diagnostic tool compared to emission spectroscopy for elucidating the interaction mechanisms in fluorescent material–biomolecule systems. When biomolecules were mixed with either **TT-TPE-TPA** or CDs, only slight, relatively insignificant deviations were observed in their PLE spectra. In contrast, the effect of biomolecules on the PLE spectrum of the conjugates was dramatic (Fig. 6). Two types of conjugates were selected for interaction studies, *i.e.* one with a low CD concentration and one with a high CD concentration. For the **TT-TPE-TPA-CN** conjugate (1 : 10 ratio), the addition of biomolecules induced an increase in emission at 535 nm within the excitation wavelength range of 375–475 nm. This observation indicates that the biomolecule stabilizes the structure of

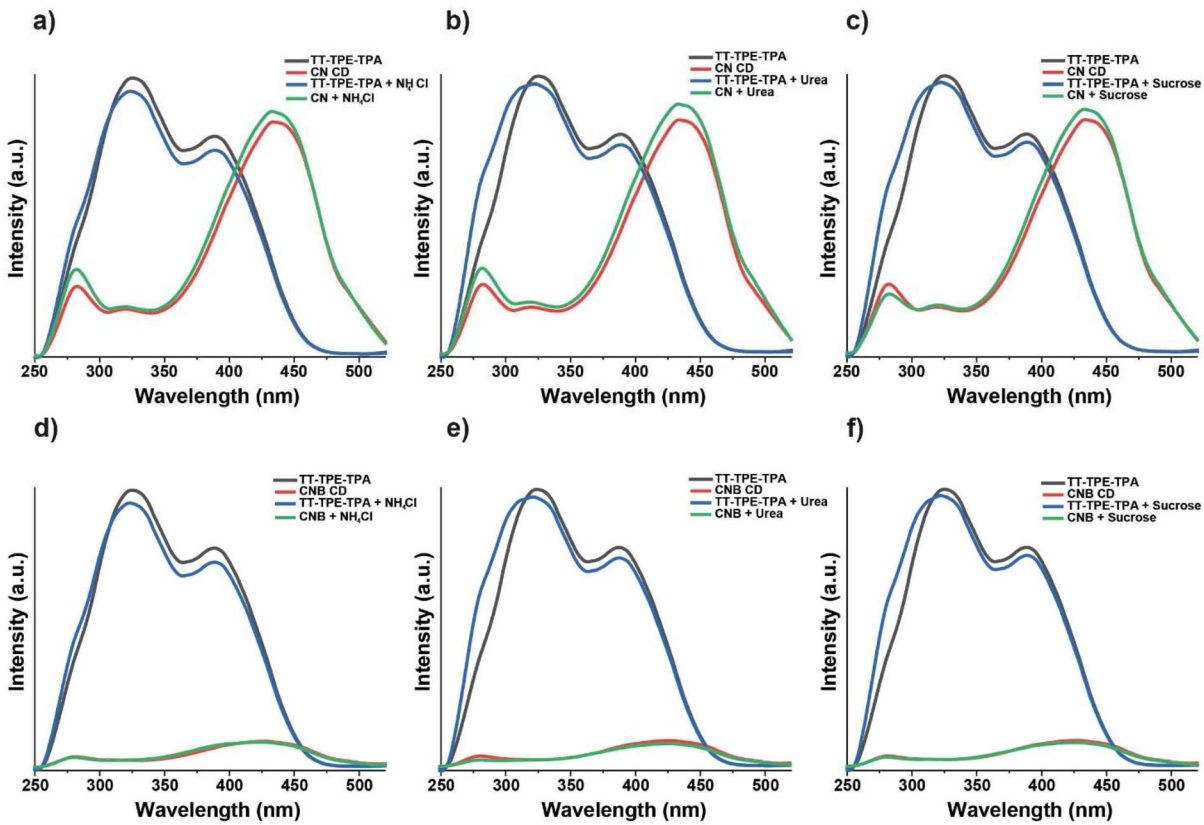

Fig. 5 Interaction of **TT-TPE-TPA** and CDs with biomolecules. The photoluminescence excitation spectrum of (a) **TT-TPE-TPA** and CN CDs with NH_4Cl. (b) **TT-TPE-TPA** and CNB CDs with NH_4Cl. (c) **TT-TPE-TPA** and CN CDs with urea. (d) **TT-TPE-TPA** and CNB CDs with urea. (e) **TT-TPE-TPA** and CN CDs with sucrose. (f) **TT-TPE-TPA** and CNB CDs with sucrose. All the photoluminescence excitation spectra were recorded at 535 nm emission.

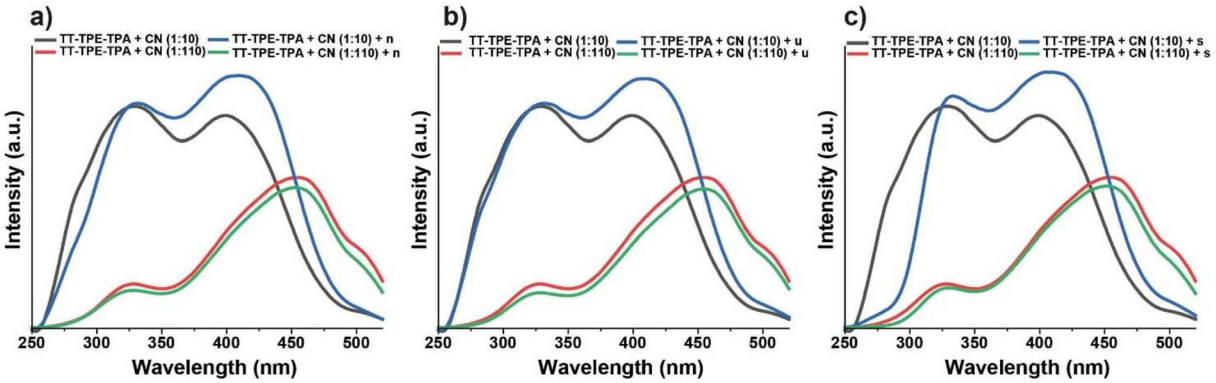

Fig. 6 Interaction of **TT-TPE-TPA-CN** CD conjugates with biomolecules. The photoluminescence excitation spectrum of (a) **TT-TPE-TPA-CN** CD conjugates with NH_4Cl (n), (b) **TT-TPE-TPA-CN** CD conjugates with urea (u), and (c) **TT-TPE-TPA-CN** CD conjugates with sucrose (s). All the photoluminescence excitation spectra were recorded at 535 nm emission.

the conjugate, thereby enhances radiative transitions. However, each biomolecule affected the 535 nm emission in the excitation wavelength range of 225–375 nm differently. In particular, urea did not alter the PLE spectrum of the **TT-TPE-TPA-CN** conjugate (1 : 10), whereas NH_4Cl caused slight quenching (5%) of the 535 nm emission in the 280–320 nm excitation range. Sucrose, in contrast, completely quenched the 535 nm emission in the 225–280 nm excitation range and significantly reduced the emission intensity in the 280–320 nm excitation range. These results suggest that NH_4Cl and sucrose interact *via* the thiophene ring, thereby facilitating a shift from radiative to nonradiative electronic transitions. Furthermore, the effect of biomolecules on the PLE spectrum of the **TT-TPE-TPA-CN** conjugate with a higher CD concentration (1 : 110 ratio) was negligible; no significant changes were observed in either the spectral shape or peak intensities. These findings indicate that an increased CD concentration inhibits the interaction between the biomolecule and the **TT-TPE-TPA-CD** conjugate.

Regarding the **TT-TPE-TPA-CBN** conjugate (1 : 10 ratio), similar to the **TT-TPE-TPA-CN** conjugate-biomolecule, the biomolecule induced an increase in emission at 535 nm within the excitation wavelength range of 375–475 nm (Fig. 7). This observation indicates that the biomolecule stabilizes the structure of the complex, thereby enhancing radiative transitions. Thus, each biomolecule affected the 535 nm emission in the excitation wavelength range of 225–375 nm differently. In particular, NH_4Cl did not alter the PLE spectrum of the **TT-TPE-TPA-CBN** conjugate (1 : 10), whereas urea and sucrose caused significant quenching (60%) of the 535 nm emission in the 280–320 nm excitation range. Moreover, urea and NH_4Cl slightly increased the emission intensity in the 280–320 nm range (8%), while sucrose slightly decreased the emission intensity in this range (6%). For the **TT-TPE-TPA-CBN** conjugate with a higher CD concentration (1 : 110 ratio), the effects of urea and NH_4Cl on the PLE spectrum were negligible; no significant changes were observed in the spectral shape or peak intensities. However, the effect of sucrose on the PLE

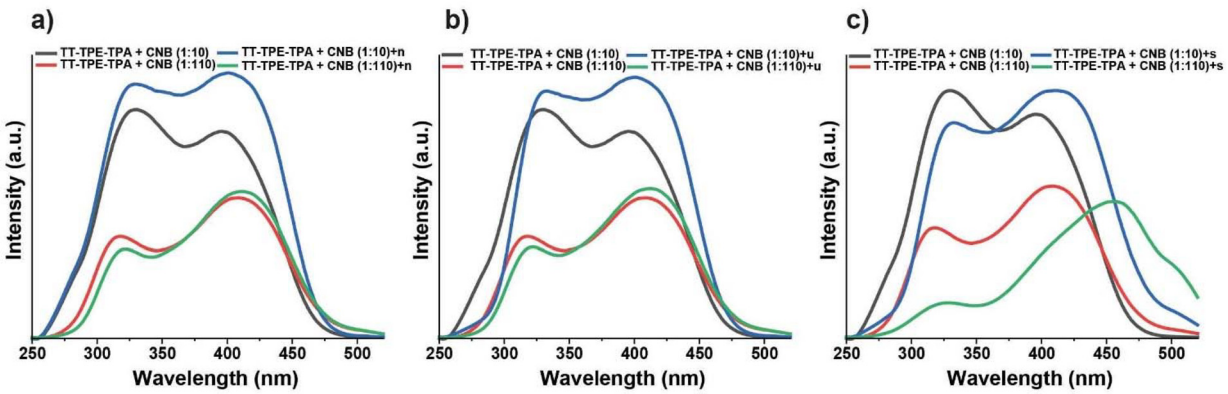

Fig. 7 Interaction of **TT-TPE-TPA-CNB** CD conjugates with biomolecules. The photoluminescence excitation spectrum of (a) **TT-TPE-TPA-CNB** CD conjugates with NH_4Cl (n), (b) **TT-TPE-TPA-CNB** CD conjugates with urea (u), and (c) **TT-TPE-TPA-CNB** CD conjugates with sucrose (s). All the photoluminescence excitation spectra were recorded at 535 nm emission.

spectrum of the high-CD conjugate was dramatic; the peak at 315 nm was significantly reduced, while the peak at 415 nm shifted to 470 nm. These results suggest that sucrose dramatically alters the structure of the conjugate, thereby modifying all electronic transitions. As sucrose is introduced, the PLE peaks associated with the CBN component become more pronounced, indicating that the electron flow is directed towards the CBN moiety and that the radiative transitions originating from CBN become more intense.

Importantly, the sucrose-induced spectral shift can be attributed to three primary factors: (i) hydrogen bonding changes, whereby sucrose can form hydrogen bonds with both water and the conjugate, modifying the local polarity and solvation environment of **TT-TPE-TPA-CBN**,[54] (ii) viscosity effects, wherein sucrose substantially increases the viscosity of solution, thereby restricting intramolecular rotations and favouring more planarized excited states that emit at different energies[55] and (iii) aggregation or micro-clustering, as sucrose can act as an osmolyte that promotes closer molecular packing or stabilizes particular conformations of the conjugates, leading to altered photophysical behaviour.[55] These mechanisms work in concert to shift the balance of radiative and nonradiative transitions and to shift the emission spectrum of conjugate. Similar phenomena were reported in related fluorophore–nanoparticle systems, where sugars or other cosolvents change the solvation shell, increase the rigidity, and induce aggregation-induced emission effects.

Collectively, these results indicate that the photophysical properties of the **TT-TPE-TPA** molecule can be controlled by forming **TT-TPE-TPA**/CD and **TT-TPE-TPA**/CD/biomolecule conjugates. Thus, our findings showed the critical role of nanomaterial–biomolecule interactions in tailoring the photophysical properties of conjugate systems. By systematically modulating the composition and concentration of **TT-TPE-TPA**, CDs and specific biomolecules, nuanced mechanisms of energy transfer, emission quenching and radiative enhancement were revealed. Moreover, the pronounced effect of sucrose in causing a bathochromic or hypsochromic shift, depending on conjugate composition, indicated how hydrogen bonding, solution viscosity and supramolecular organization together effect the photophysical properties. These insights not only advance our fundamental understanding of nanoscale interactions but also enable researchers to design highly sensitive and tunable optical probes for biosensing, imaging and other advanced technological applications.

4. Conclusion

A highly fluorescent thienothiophene fluorophore, **TT-TPE-TPA**, was designed and synthesized for the first time as a QD conjugate. Its photophysical properties were investigated by UV-Vis and fluorescence spectroscopies. Carbon–nitrogen (CN) and carbon–nitrogen–boron (CNB) dots of **TT-TPE-TPA** were successfully prepared. The photophysical characteristics of **TT-TPE-TPA** can be precisely modulated through its conjugation with carbon dots and further influenced by specific biomolecular interactions. By varying the concentration and composition of these conjugates, distinct shifts in radiative and nonradiative transitions of **TT-TPE-TPA** were observed. Moreover, the differential effects of biomolecules like urea, sucrose and NH_4Cl revealed that the nano-bio interface can be strategically tuned to either stabilize or disrupt electronic transitions of **TT-TPE-TPA**. These observations showed that the development of highly sensitive and customizable optical probes for biosensing, imaging and optoelectronic applications is achievable through the design of conjugates with **TT-TPE-TPA** and CDs/biomolecules. We hope that this work inspires additional investigation of fluorescent nanomaterials in highly tunable and promising systems of TT and QD.

Author contributions

Recep Isci: supervision, investigation, writing – review & editing, data curation and writing – original draft. Ozge Ibis: investigation, writing – review & editing and data curation. Garen Suna: investigation and data curation. Caner Unlu: supervision, investigation, writing – review & editing, data curation and writing – original draft. Turan Ozturk: supervision, investigation, writing – review & editing, data curation and writing – original draft.

Data availability

The authors confirm that the data supporting the findings of this study are available within the article and its Supporting material. Raw data that support the findings of this study are available from the corresponding author, upon reasonable request.

Conflicts of interest

The authors declare no conflict of interest.

Acknowledgements

We thank Istanbul Technical University (ITU), TGA-2023-44077, TDA-2024-45680, TYLB-2023-45051, PTA-2024-45861, FHD-2024-45962 numbered ITU BAP projects, 124Z353 numbered TUBITAK 1001 Project, and Unsped Global Lojistik, Turkey, for financial support.

References

1 M. Haase and H. Shafer, *Angew. Chem., Int. Ed.*, 2011, **50**, 5808–5829.

2 I. L. Medintz, H. T. Uyeda, E. R. Goldman and H. Mattoussi, *Nat. Mater.*, 2005, **4**, 435–446.
3 A. Cirpan and F. E. Karasz, *J. Appl. Polym. Sci.*, 2006, **99**, 3125–3129.
4 S. M. Tawfik, M. Sharipov, S. Kakhkhorov, M. R. Elmasry and Y.-I. Lee, *Adv. Sci.*, 2019, **6**, 1801467.
5 M. A. Hejazi, I. Y. Coskun, F. Y. Unlu, A. Aydogan, C. Unlu and L. Trabzon, *Diamond Relat. Mater.*, 2024, **148**, 111438.
6 E. Budak, S. Aykut, M. E. Pasaoglu and C. Unlu, *Mater. Today Commun.*, 2020, **24**, 100975.
7 X. Chen, W. Wu, W. Zhang, Z. Wang, Z. Fu, L. Zhou, Z. Yi, G. Li and L. Zeng, *Appl. Phys. Lett.*, 2021, **118**, 153102.
8 J. Kong, Y. Wei, F. Zhou, L. Shi, S. Zhao, M. Wan and X. Zhang, *Molecules*, 2024, **29**, 2002.
9 S. Bhandari, D. Mondal, S. K. Nataraj and R. G. Balakrishna, *Nanoscale Adv.*, 2019, **1**, 913–936.
10 R. Das, R. Bandyopadhyay and P. Pramanik, *Mater. Today Chem.*, 2018, **8**, 96–109.
11 M. Han, S. Zhu, S. Lu, Y. Song, T. Feng, S. Tao, J. Liu and B. Yang, *Nanotoday*, 2018, **19**, 201–218.
12 O. Ibis, N. Uk, I. Nar and C. Unlu, *Spectrochim. Acta, Part A*, 2025, **327**, 125348.
13 S. D. Hiremath, A. Thakuri, M. M. Joseph, A. A. Bhosle, K. K. Maiti, M. Banerjee and A. Chatterjee, *ACS Appl. Nano Mater.*, 2023, **6**(11), 9958–9967.
14 B. Saboorizadeh and R. Z.- Dorabei, *ACS Biomater. Sci. Eng.*, 2022, **8**(8), 3589–3595.
15 P. Zhu, Y. Gan, K. Lin, C. Lin, S. Li, S. Yu and J. Shi, *ACS Omega*, 2020, **5**(9), 4482–4489.
16 L. Liang, X. Peng, F. Sun, Z. Kong and J.-W. Shen, *Nanoscale Adv.*, 2021, **3**, 904–917.
17 X. Feng, F. Zhang, Y. Wang, Y. Zhang, Y. Yang and X. Liu, *J. Electron. Mater.*, 2016, **45**, 2784–2788.
18 E. Rusen, A. Diacon, A. Mocanu, R. Gavril, L. C. Nistorc and A. Dinescu, *RSC Adv.*, 2016, **6**, 25577.
19 C. Zhao, C. Zhu, Y. Yu, W. Xue, X. Liu, F. Yuan, J. Dai, S. Wang, B. Jiao and Z. Wu, *ACS Appl. Mater. Interfaces*, 2023, **15**(33), 40080–40087.
20 P. Sehgal and A. k. Narula, *Opt. Mater.*, 2015, **48**, 44–50.
21 B. Amna, R. Isci, S. Faraji, H. M. Siddiqi and T. Ozturk, *Org. Electron.*, 2024, **135**, 107147.
22 R. Isci, H. Bildirir, D. Gunturkun, M. G.- Mendoza, M. Liras, V. A. de la P. O'Shea and T. Ozturk, *J. Mater. Chem. C*, 2024, **12**, 16108–16119.
23 R. Isci, D. Gunturkun, A. S. Yalin and T. Ozturk, *J. Polym. Sci.*, 2021, **59**, 117–123.
24 R. Isci, L. Wan, S. Topal, D. Gunturkun, A. J. Campbell and T. Ozturk, *J. Mater. Chem. C*, 2022, **10**(29), 10719–10727.
25 R. Isci, T. Balkan, S. Tafazoli, B. Sütay, M. S. Eroglu and T. Ozturk, *ACS Appl. Energy Mater.*, 2022, **5**, 13284–13292.
26 S. E. Ozturk, R. Isci, S. Faraji, B. Sütay, L. A. Majewski and T. Ozturk, *Eur. Polym. J.*, 2023, **191**, 112028.
27 D. Gunturkun, R. Isci, B. Sütay, L. A. Majewski, S. Faraji and T. Ozturk, *Eur. Polym. J.*, 2022, **170**, 111167.
28 D. Gunturkun, R. Isci, S. Faraji, B. Sütay, L. A. Majewski and T. Ozturk, *J. Mater. Chem. C.*, 2023, **11**(38), 13129–13141.
29 M. E. Cinar and T. Ozturk, *Chem. Rev.*, 2015, **115**(9), 3036–3140.
30 B. Amna, R. Isci, H. M. Siddiqi, L. A. Majewski, S. Faraji and T. Ozturk, *J. Mater. Chem. C*, 2022, **10**(21), 8254–8265.
31 R. Isci and T. Ozturk, *Beilstein J. Org. Chem.*, 2023, **19**, 1849–1857.
32 R. Isci and T. Ozturk, *Turk. J. Chem.*, 2023, **47**(5), 1239–1248.
33 A. Suerkan, R. Isci, T. Ozturk and Y. Yagci, *Mol. Syst. Des. Eng.*, 2023, **8**(10), 1319–1326.
34 R. Isci, K. B. Donmez, N. Karatepe and T. Ozturk, *ACS Appl. Energy Mater.*, 2024, **7**(4), 1488–1494.
35 R. Isci, E. Baysak, G. Kesan, B. Minofar, M. S. Eroglu, O. Duygulu, S. F. Gorkem and T. Ozturk, *Nanoscale*, 2022, **14**, 16602–16610.
36 E. Karakus, S. Gunduz, L. Liv and T. Ozturk, *J. Photochem. Photobiol., A*, 2020, **400**, 112702.
37 R. Isci, A. R. Varzeghani, K. Kaya, B. Sütay, E. Tekin and T. Ozturk, *ACS Sustainable Chem. Eng.*, 2022, **10**(4), 1605–1615.
38 J. Wang, K. Liu, L. Ma and X. Zhan, *Chem. Rev.*, 2016, **116**, 14675–14725.
39 R. Isci, M. Unal, T. Yesil, A. Ekici, B. Sütay, C. Zafer and T. Ozturk, *Front. Mater.*, 2023, **10**, 1125462.
40 R. Isci, M. Unal, G. Kucukcakir, N. A. Gurbuz, S. F. Gorkem and T. Ozturk, *J. Phys. Chem. B*, 2021, **125**, 13309.
41 R. Isci, E. Tekin, K. Kaya, S. P. Mucur, S. F. Gorkem and T. Ozturk, *J. Mater. Chem. C*, 2020, **8**, 7908–7915.
42 L. Bian, Y. Liang and Z. Liu, *ACS Appl. Nano Mater.*, 2022, **5**(10), 13940–13958.
43 R. Isci, E. Tekin, S. P. Mucur and T. Ozturk, *ChemistrySelect*, 2020, **5**, 13091–13098.
44 R. Isci, B. C. Sadikogullari, B. Sütay, B. Karagoz, A. D. Ozdemir and T. Ozturk, *J. Photochem. Photobiol., A*, 2025, **459**, 116095.
45 O. Sahin, M. E. Cinar, E. Tekin, S. P. Mucur, S. Topal and G. Suna, *ChemistrySelect*, 2017, **2**, 2889–2894.
46 R. Isci, E. Gencosman, Y. Yagci and T. Ozturk, *J. Photochem. Photobiol., A*, 2024, **449**, 115427.
47 E. Budak, D. Erdogan and C. Unlu, *Photosynth. Res.*, 2021, **147**, 1–10.
48 G. I. Makhatadze and P. L. Privalov, *J. Mol. Biol.*, 1992, **226**, 491–505.
49 N. Das, E. Tarif, A. Dutta and P. Sen, *J. Phys. Chem. B*, 2023, **127**(14), 3151–3163.
50 K. A. Dill, *Biochemistry*, 1990, **29**(31), 7133–7155.
51 R. Nassar, G. L. Dignon, R. M. Razban and K. A. Dill, *J. Mol. Biol.*, 2021, **433**(20), 167126.
52 D. W. Bolen and G. D. Rose, *Annu. Rev. Biochem.*, 2008, **77**, 339–362.
53 M. T. Record Jr, W. Zhang and C. F. Anderson, *Adv. Protein Chem.*, 1998, **51**, 281–353.

54 D. P. Surzhikova, L. A. Sukovatyi, E. V. Nemtseva, E. N. Esimbekova and E. A. Slyusareva, *Micromachines*, 2023, **14**, 1442.

55 M. M. Sreejaya, V. M. Pillai, A. Ayesha, M. Baby, M. Berab and M. Gangopadhyay, *J. Mater. Chem. B*, 2024, **12**, 2917–2937.